frontiers | Frontiers in Nanotechnology

TYPE Original Research
PUBLISHED 23 December 2024
DOI 10.3389/fnano.2024.1516133

OPEN ACCESS

EDITED BY
Rongzhi Chen,
University of Chinese Academy of Sciences, China

REVIEWED BY
Sharanabasava V. Ganachari,
KLE Technological University, India
Anirban Kundu,
Anthesis Group, Canada

*CORRESPONDENCE
Anis Ahmad Chaudhary,
aachaudhary@imamu.edu.sa
Nadeem Raza,
nrmostafa@imamu.edu.sa,
nadeemr890@gmail.com

RECEIVED 23 October 2024
ACCEPTED 29 November 2024
PUBLISHED 23 December 2024

CITATION
Ali Z, Raza N, Hayat M, Khezami L, Khairy M, Almuqri EA, Basher NS, Parveen H and Chaudhary AA (2024) Synthesis and characterization of a fluorescent magnetic molecularly imprinted polymer for enhanced adsorption and selective extraction of pesticides from agricultural waters.
Front. Nanotechnol. 6:1516133.
doi: 10.3389/fnano.2024.1516133

Synthesis and characterization of a fluorescent magnetic molecularly imprinted polymer for enhanced adsorption and selective extraction of pesticides from agricultural waters

Zeeshan Ali[1], Nadeem Raza[2]*, Muhammad Hayat[1], Lotfi Khezami[2], Mohamed Khairy[2], Eman Abdullah Almuqri[3], Nosiba S. Basher[3], Humaira Parveen[4] and Anis Ahmad Chaudhary[3]*

[1]Institute of Chemical Sciences, Bahauddin Zakariya University, Multan, Pakistan, [2]Department of Chemistry, College of Science, Imam Mohammad Ibn Saud Islamic University (IMSIU), Riyadh, Saudi Arabia, [3]Department of Biology, College of Science, Imam Mohammad Ibn Saud Islamic University (IMSIU), Riyadh, Saudi Arabia, [4]Department of Chemistry, Organic and Medicinal Chemistry Research Lab., Faculty of Science, University of Tabuk, Tabuk, Saudi Arabia

Introduction: A novel fluorescent magnetic molecularly imprinted polymer (FMMIP) was developed for the effective extraction of malathion (MLT) and chlorpyrifos (CPS) from agricultural water sources.

Methods: The FMMIP was confirmed to have a stable polymer structure with significant thermal resilience through comprehensive characterization using techniques such as TEM and TGA. The magnetic properties of the FMMIP facilitated easy separation by external magnetic fields, with a notable magnetization of 0.006 emu/g. Kinetic and isotherm studies revealed that adsorption of MLT and CPS onto the FMMIP conformed best to the pseudo-first-order model and Freundlich isotherm, suggesting a predominance of physisorption mechanisms and heterogeneous binding sites.

Results and Discussion: The FMMIP demonstrated exceptional adsorption capacities, achieving a maximum of 93 mg/g for MLT and 69 mg/g for CPS. Regeneration trials indicated that the FMMIP maintains its high adsorptive performance over multiple cycles, highlighting its potential for sustainable use. Statistical validation confirmed the method's reliability, with RSD values for MLT and CPS at 6.5% and 7.3%, respectively, and LODs determined to be 1.26 mg/L for MLT and 1.22 mg/L for CPS. The strong R^2 values of 0.992 for MLT and 0.998 for CPS from the adsorption studies substantiate the method's effectiveness. This study demonstrates that the synthesized FMMIP is a promising material for removing MLT and CPS, supporting its application in environmental clean-up initiatives to protect and preserve ecosystems.

KEYWORDS

molecularly imprinted polymer, selective recognition, malathion, chlorpyrifos, agricultural water, adsorption kinetics

1 Introduction

In recent years, substantial industrial growth has badly polluted the natural ecosystem since many agro-based industries discharge residuals agrochemicals such as fertilizers, fungicides, and pesticides as effluents, which potentially contaminate water sources and soil, leading to severe threats to animals and humans (Assafi et al., 2023; Dhananjayan et al., 2020; Gul et al., 2024). Pesticides and insecticides are associated with health issues ranging from acute to chronic conditions. These include cancer, neurotoxicity, and endocrine disruption (Encarnação et al., 2019). Among diverse insecticides, malathion (MLT) and chlorpyrifos (CPS) are commonly used to control insects on fruits and vegetables.

Malathion is an organophosphate insecticide commonly used as a spray or mist to control insects such as mosquitoes, flies, fleas, ants, and several other insects in agricultural and residential settings (Liu et al., 2004). It works by inhibiting the activity of acetylcholinesterase enzyme, which is necessary for proper nerve function in insects (and also in humans). Inhibition of this enzyme by MLT leads to paralysis and subsequent death in target insects (Sharma et al., 2020). However, MLT can also be toxic to non-target species, including humans, pets, and wildlife, if it is not handled correctly or if safety guidelines are not observed (Rey et al., 2012). Therefore, it is imperative to use malathion with caution and follow the instructions on the label (Bharti and Rasool, 2021).

Chlorpyrifos belongs to the organophosphate class of chemicals and is a widely used pesticide to control insects and pests in agriculture (Ata et al., 2013). Chlorpyrifos also inhibits the activity of acetylcholinesterase and raises the level of acetylcholine, leading to overstimulation of the nervous system and, ultimately, the paralysis and death of the target insect (Rahman et al., 2021). Although chlorpyrifos is effective in pest control, it has been linked to several health and environmental concerns. Studies have shown that exposure to CPS can cause acute and chronic health effects, including neurological effects, developmental delays, and immune system suppression (Rahman et al., 2021). It is also highly toxic to non-target organisms, including birds, fish, and bees, and can persist in the environment for a long time (Hashimi et al., 2020). Considering the severe concerns linked with CPS, several countries have banned or restricted its use due to its strong potential to cause severe health and environmental concerns (Coria and Elqueta, 2022).

Molecular imprinting technology has been recognized as a promising technique for monitoring and removing agrochemicals contained in environmental samples (Monsalve-Atencio et al., 2022). Molecular imprinting technology employs synthetic polymeric materials tailor-made to selectively bind target molecules, such as agrochemicals, according to their size, shape, and functional groups (Hasanah et al., 2021). Fabricating molecularly imprinted polymers (MIPs) involves using a template molecule that structurally resembles the target molecule (Villa et al., 2021). The template is mixed with monomers and cross-linking agents to form a cross-linked polymer network exhibiting cavities, or "imprints," that are complementary in size, shape, and functionality to the template molecule (Mrozek et al., 2010). The fabricated MIP can selectively bind to the target molecule due to the specific recognition sites created during the polymerization process. To this note, MIPs have become a powerful tool for detecting and removing agrochemicals as they can be tailored to specifically recognize and capture target molecules while leaving other non-target molecules intact. For example, Zuo et al., synthesized MIP for the removal of Malathion from agricultural waste (Zuo et al., 2015). In another study Urucu et al., deployed molecularly imprinted solid-phase extraction for the determination of Chlorpyrifos in water samples (Urucu et al., 2020). Furthermore, MIPs have many potential applications including separation and purification, sensing and detection, drug delivery, catalysis, environmental remediation, food analysis, and biomedical applications (Zarei and Zarei, 2018; Han et al., 2022). However, further modification of MIPs with some nanoparticles exhibiting magnetic properties such as magnetite (Fe_3O_4) can augment their performance as the resulting materials could be used to selectively recognize and capture target molecules in complex biological matrices such as extracts of plant vegetables and fruits (Ansari and Karimi, 2017).

Contrary to conventional pesticide removal techniques, fluorescent magnetic molecularly imprinted polymers (FMMIPs) offer several advantages. The high specificity of MIPs for target molecules significantly reduces the likelihood of false positives or negatives (Ali and Omer, 2022). Incorporation Fe_3O_4 particles facilitates the swift magnetic separation of bound molecules from the sample matrix. Additionally, the fluorescein-5-isothiocyanate (FITC) coating on the core shell imparts luminescence, enabling easier identification during analytical procedures. Adopting MIPs also diminishes the necessity for costly and labor-intensive purification steps, enhancing the efficiency and cost-effectiveness of the target removal process (Akgönüllü and Denizli, 2022). This study aimed to develop an MIP-based material using non-toxic chemicals that features dual recognition sites for the selective extraction of Malathion (MLT) and Chlorpyrifos (CPS). A further goal was to engineer a material that was easily separable and detectable throughout the analysis. The findings of this research could contribute to water treatment processes and the preservation of natural ecosystems. The schematic illustration for FMMIP synthesis and its application for sample analysis is given in Figure 1.

2 Experimental

2.1 Reagents and materials

Iron (III) chloride hexahydrated ($FeCl_3.6H_2O$) 98%, Iron (II) sulfate ($FeSO_4.7H_2O$) 99.5%, tri-sodium citrate ($Na_3C_6H_5O_7$) 99.0%, tetraethyl orthosilicate (TEOS) 99.99%, ammonia solution 25%, acetone, ethanol 99.7%, fluorescein-5-isothiocyanate (FITC), 3-aminopropyltriethoxysilane (APTS vol) < 98%, dopamine hydrochloride 99%, 2-amino-2-(hydroxymethyl)1,3 propanediol (Tris) 99%, hydrochloric acid (HCl) 38%. All the chemicals were purchased from Sigma Aldrich and Merck and were used without further purification. Malathion 90%, and Chlorpyrifos 97% were purchased from Hebei Hontai Biotech Co., Ltd., China and Shanghai Molotus Chemical Co., Ltd, China, respectively.

2.2 Synthesis of Fe_3O_4 nanoparticles

A previously published procedure was used to synthesize the Fe_3O_4 nanoparticles by co-precipitating iron (II) and iron (III) salts

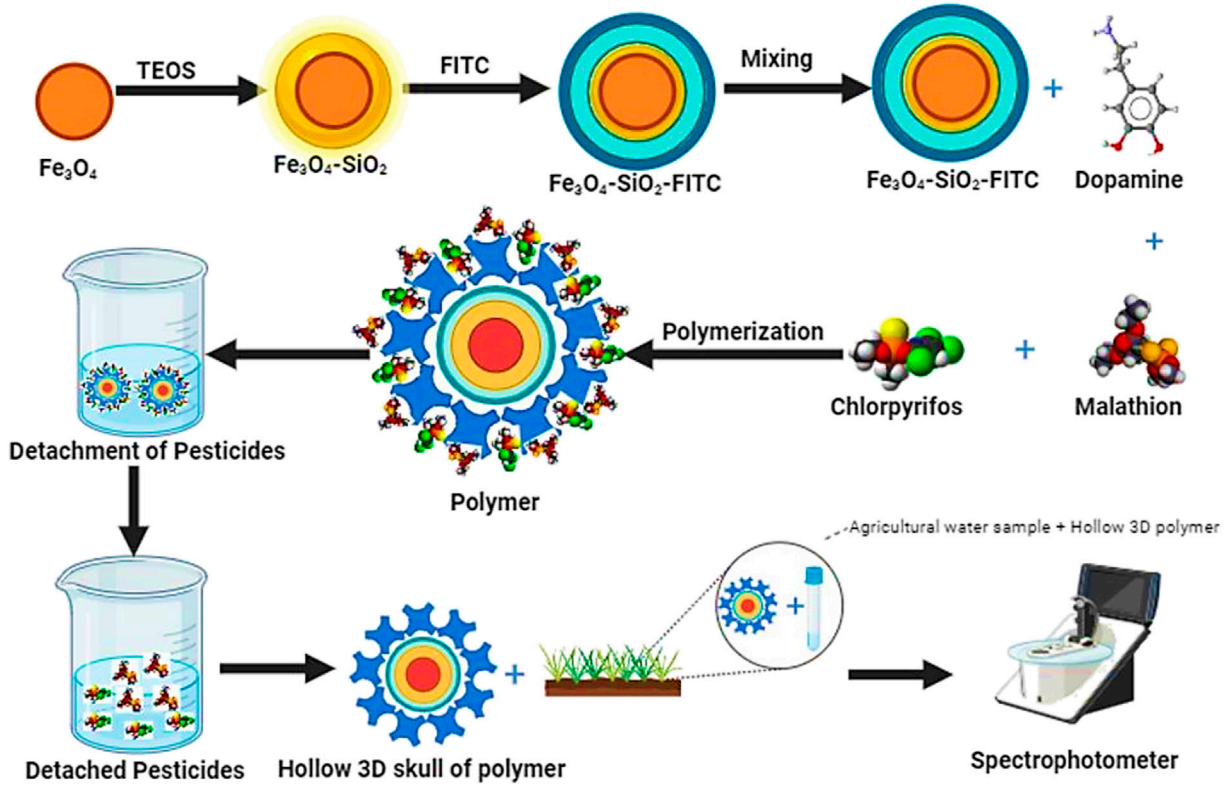

FIGURE 1
Graphical illustration of synthesis of FMMIP and its application in adsorption of target pesticides from agriculture run-off.

in a 1:2 molar ratio. Specifically, a two-necked round-bottom flask containing 10 mmol of iron sulphate and 20 mmol of iron chloride in 100 mL of deionized water under N_2 atmosphere was heated at 70°C for 30 min. Then, 33 mL of 25% ammonia solution was poured into the above mixture until a brownish-black precipitate of iron oxide nanoparticles was formed and rinsed with distilled water and ethanol until pH 7 is attained. The resultant product was separated using an external magnetic field and vacuum-dried for 24 h at room temperature. To modify the surface of iron oxide nanoparticles, the synthesized nanoparticles were re-dispersed in 200 mL of deionized water containing 0.3 M sodium citrate and heated at 60°C for 2 h. After washing the nanoparticles with acetone to get rid of any remaining citrate, they were dried for 15 h in a vacuum desiccator.

2.3 Coating of TEOS

Silica coating on Fe_3O_4 nanoparticles (NPs) was executed by following a previously published method to prevent aggregation and enhance the stability of NPs (Kralj et al., 2010). In a sonication tub, Fe_3O_4 nanoparticles were dispersed in 50 mL of deionized water. A mixture of ammonia solution 25% (5 mL) and ethanol (140 mL) was poured into an aliquot of 2 mL of water-dispersed iron nanoparticles, followed by dilution with 40 mL of deionized water and stirred for 18 h. A solution of 20 mL of ethanol and 1 mL of TEOS was gradually added into the above-diluted ferrofluid and was kept at room temperature for 16 h. The final product was separated using an external magnetic field, rinsed with ethanol and distilled water several times, and dried in a vacuum desiccator.

2.4 Construction of fluorescent layer on silica-coated iron nanoparticles

The silica-coated fluorescent nanoparticles (Fe_3O_4-SiO_2-FITC nanoparticles) were synthesized using the protocol described in a recent study (Asadi et al., 2016). Briefly, 0.04 g of FITC was mixed in 10 mL of ethanol and 0.22 mL of APTS, and the resultant solution was stirred for 24 h in the dark by wrapping the flask with aluminum foil. Fe_3O_4-SiO_2 nanoparticles were added to the above FITC solution, and the mixture was mechanically agitated for 15 h. Fluorescent silica-coated iron nanoparticles (Fe_3O_4-SiO_2-FITC) were separated from the mother liquor with the help of an applied magnetic field and then dried in a vacuum at room temperature.

2.5 Synthesis of FMMIPs and MNIPs (magnetic non imprinted polymers)

Free radical polymerization was used to synthesize the FMMIPs (Yin et al., 2015). Using this approach, 40 mg of tris buffer (2-amino-2-hydroxymethyl 1, 3 propanediol) dissolved in 50 mL deionized water at pH 11 was mixed with 80 mg of fluorescent silica-coated iron nanoparticles, 80 mg of dopamine hydrochloride as a

monomer, and 15 mg of each target pesticide (MLT and CPS). The pH of the above solution was reduced to 8.5 by adding concentrated HCl dropwise and leaving this reaction to continue at room temperature (25°C) for 16 h to ensure the polymerization process. Target pesticides (MLT and CPS) attached on FMMIPs surface with hydrogen bonding and π-π interaction due to functionalities developed on polymeric surface. The FMMIPs thus formed was separated using an external magnetic field and rinsed three times with distilled water and ethanol to remove any unbound pesticide. To prepare FMNIPs, the same protocol was adopted as for FMMIPs, but in the absence of pesticide (template).

2.6 Adsorption experiments

The maximum absorption wavelengths (λ_{max}) for MLT and CPS were determined using a UV-Vis spectrophotometer across the range of 200–400 nm, with MLT and CPS concentrations in solutions being measured at their respective λ_{max} of 230–254 nm. To initiate the experiment, 50 mL of a 50 mg L^{-1} standard solution of MLT and CPS was added to each of the 32 test tubes. At the time of analysis, the sample was filtered using a membrane filter paper (pore size 0.45 μm, diam. 47 mm) to remove any remining suspended particles. Subsequently, 50 mg of FMMIP was introduced to 16 of these test tubes, while the remaining 16 received 50 mg of FMNIP. Aliquots were sampled at predetermined intervals (5, 10, 15, 20, 25, 30, 35, and 40 min) to determine the binding capacity (q_e). A gradient of standard solutions of MLT and CPS, with concentrations ranging from 10 to 100 mg L^{-1}, was prepared for subsequent adsorption experiments conducted at room temperature. For each concentration, 50 mL of the solution was combined with 50 mg of FMMIP in a separate test tube. These mixtures were then agitated on a shaker for 30 min at room temperature to reach equilibrium. The solutions were filtered through an HPLC-grade filter (0.45 μm) after agitation. An identical procedure was applied using FMNIP. After separation, the pesticides bound to FMMIP (FMMIP-MLT/CPS complexes) were eluted using an ethanol-water solution (8:2 v/v) in a 100 μL pipette tip at a flow rate of 10 μL min^{-1}. A UV-Vis spectrophotometer quantified the concentrations of the eluted pesticides. The binding capacity of the spiked samples was determined using Equation 1.

$$qe = \frac{(Ci - Cf)}{M} \times V \quad (1)$$

Where q_e is the binding capacity, C_i and C_f are the respective initial and final concentrations of the analyte in solution, V and M represents the solution volume, an FMMIP mass. Further, the effect of pH on the binding capacity of FMMIP was evaluated.

2.7 Sample analysis in agricultural run-off water samples

To assess the efficacy of FMMIP 1L of agricultural water sample was collected from the vicinity of agricultural land near Multan district and stored in previously cleaned glass bottles at 5°C. Water samples were firstly filtered through Whatmann filter paper and then a membrane filter paper (pore size 0.45 μm, diam. 47 mm) was employed to remove suspended particulates. The pH was then adjusted to a neutral value of 7. Three separate 40 mL aliquots of water, contained in different beakers, were spiked with MLT and CPS at concentrations of 0.01, 15, and 30 mg L^{-1}. These spiked samples were subsequently subjected to analysis using the previously described method.

2.8 Regeneration study

The regeneration of an adsorbent is critical for its practical applications. For this purpose, the sample solution was prepared by adding 20 mg of FMMIP in 15 mg L^{-1} of the target pesticides; MLT and CPS at room temperature. The mixture was stirred for 30 min at 100 rpm and then filtered through HPLC grade filter with a pore size of 0.45 μm and the concentration of the target pesticides in the filtered solution was measured using a UV-vis spectrophotometer at their respective wavelengths (230 nm for MLT and 245 nm for CPS). Afterwards, the absorbent was separated, washed with distilled water and ethanol, and dried at 100°C. The regenerated FMMIP was used in five consecutive adsorption-desorption cycles.

2.9 Characterization

The presence of functional groups in FMMIPs and their unmodified components was detected by Attenuated Total Reflection (ATR) infrared spectra, which were recorded using a Perkin-Elmer FT-IR (Thermo Scientific) within the spectral range of 4,000 to 500 cm^{-1} at a resolution of 4 cm^{-1} and a scan rate of 16 scans per second. The UV-Vis absorption spectra were acquired with a Cary 60 UV-Vis spectrophotometer (Agilent Technologies). The surface morphology of the FMMIPs and individual components was visualized using a Scanning Electron Microscope (SEM LEO 1560, Zeiss, Oberkochen, Germany) operated at 10 kV and a Transmission Electron Microscope (TEM, Tecnai Spirit BioTWIN, FEI Company, Oregon, United States) operated at 20–120 kV. Thermal Gravimetric Analysis (TGA) was performed on the iron nanoparticles, core-shell, and FMMIP using a TGA Q5000 V3.17 Build 265 instrument, with the samples being heated for 30 min at 900°C to evaluate their thermal properties.

3 Results and discussion

3.1 FT-IR

The FT-IR spectra depicted in Figure 2 demonstrate the characteristic functional groups of various nanomaterials: Fe_3O_4 nanoparticles (NPs), silica-coated Fe_3O_4 (Fe_3O_4-SiO_2) with fluorescein isothiocyanate (FITC), and FMMIPs complexed with MLT and CPS. The spectra for Fe_3O_4 NPs exhibit distinct peaks at 631 and 577 cm^{-1}, attributed to the Fe-O stretching vibrations, confirming the presence of iron oxide (Figure 2A). In the core-shell spectrum (Figure 2B), the peaks at 1,078, 800, and 1727 cm^{-1} are assigned to Si-O-Si stretching vibrations, Si-O symmetric stretching, and the carbonyl group characteristic of lactones, respectively, while the peak at 2015 cm^{-1} indicates the isothiocyanate group. These

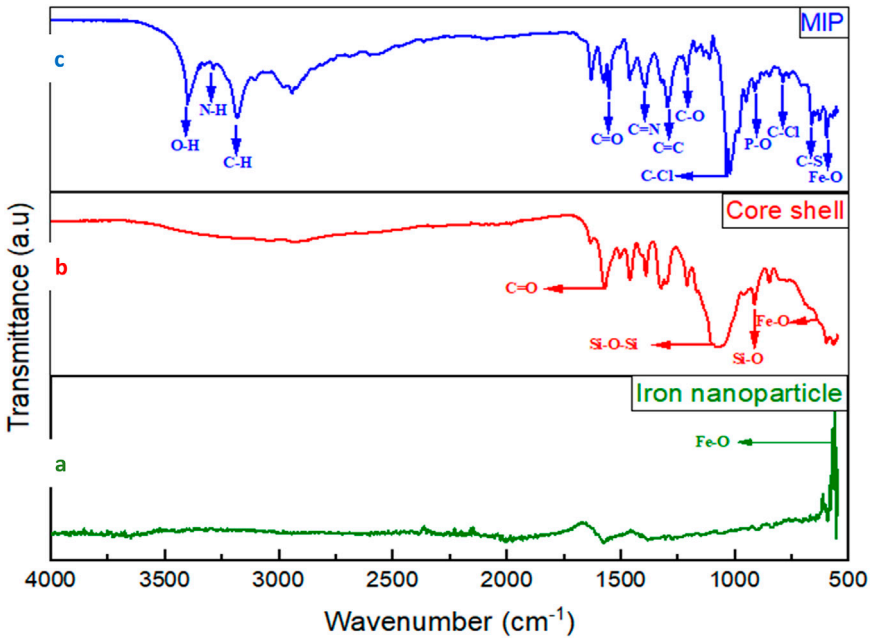

FIGURE 2
The FT-IR spectrum of the FMMIP alongside its components: **(A)** iron nanoparticle, **(B)** core-shell, and **(C)** pesticide-loaded FMMIP.

peaks verify the successful coating of silica and FITC on the Fe_3O_4 nanoparticles. The FMMIP spectrum (Figure 2C), the broad bands around 3,600, 3,400, and 2,900 cm^{-1} correspond to O-H, N-H, and C-H stretching vibrations, suggesting MLT, CPS, and polydopamine incorporation. The pronounced peaks at 1720, 1,690, and 1,631 cm^{-1} are associated with C=C, C=N, and C=O conjugations, respectively. Additional peaks at 1715, 1,655, 1,211, 980, 778, 730, and 577 cm^{-1} indicate the ester and amide functionalities, C-Cl stretching, P-O-C, and S-C bending vibrations, alongside the characteristic Fe-O stretch of Fe_3O_4. These spectral features are conclusive evidence of the successful synthesis of FMMIP nanoparticles.

3.2 Microscopic studies

The morphological features of the synthesized FMMIP and their foundational components; including Fe_3O_4 nanoparticles and silica-coated Fe_3O_4 (core-shell), are presented in Figures 3A–C. The particle size distributions of these materials are given in Supplementary Figure S1. The Fe_3O_4 nanoparticles exhibited an average diameter of approximately 60–70 nm with minimal agglomeration (Bojdi et al., 2016; Ali et al., 2022). After the modification with Tetraethyl orthosilicate (TEOS), the Fe_3O_4-SiO_2 nanoparticles displayed an increased average size of 118 nm, indicating successful coating of silica shell. The FMMIPs, when further coated with polydopamine, demonstrated an increase in size to around 250 nm, authenticating the successful fabrication of the FMMIP. The smooth surface of FMMIP confirms the successful polymerization process. Transmission electron microscopy (TEM) analysis provided additional verification of the polydopamine layer on the silica core-shell laden with MLT and CPS, as depicted in Figure 3D. The particle sizes of the various nanomaterials were measured using ImageJ1.52v software with Java 1.8.0_112 (64-bit).

3.3 Magnetic study

The magnetic behaviors of Fe_3O_4 nanoparticles, silica-coated Fe_3O_4 (Fe_3O_4-SiO_2), and pesticide-loaded FMMIP were investigated using a vibrating sample magnetometer (VSM), as depicted in Figure 4. The Fe_3O_4 nanoparticles exhibited the highest magnetization value, attributed to their pure magnetic composition. The magnetization of the core-shell nanoparticles decreased due to the TEOS and FITC coatings. A further decrease in saturation magnetization was observed for FMMIP, which can be attributed to the incorporation of non-magnetic layers such as the polydopamine coating and the pesticide loading on the core-shell structure (Fe_3O_4-SiO_2-FITC). Nevertheless, the FMMIP nanoparticles retained sufficient magnetic responsiveness to be manipulated by an external magnetic field (Ali et al., 2023).

3.4 TGA analysis

Thermogravimetric analysis was performed to evaluate the content of magnetite and the extent of cross-linking within the imprinted polymer coatings of the synthesized nanomaterials. Figure 5 illustrates the thermogravimetric weight loss profiles for the iron nanoparticle, silica core-shell, and pesticide-loaded FMMIP.

The TGA curves for Fe_3O_4 nanoparticles, Fe_3O_4-SiO_2-FITC nanocomposites, and FMMIPs are presented in Figures 5A–C. The thermogram for Fe_3O_4 (Figure 5A) exhibited a weight loss of approximately 15% around 280°C, attributed to the desorption of

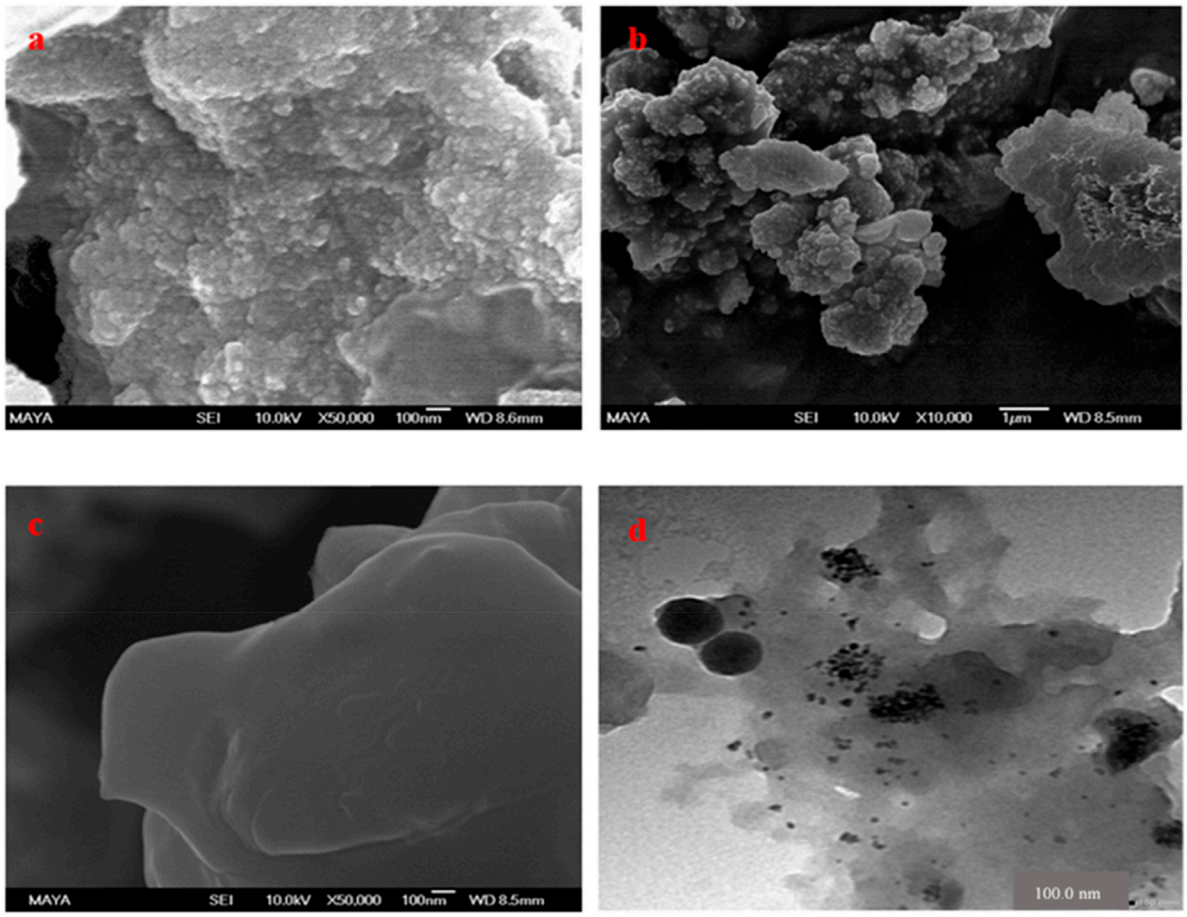

FIGURE 3
SEM images of **(A)** iron nanoparticles, **(B)** silica coated core shell, **(C)** FMMIPs loaded with MLT and CPS and TEM image of **(D)** FMMIPs loaded with MLT and CPS.

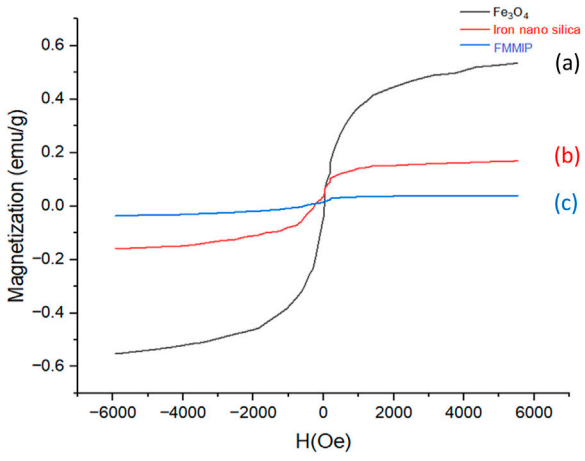

FIGURE 4
Magnetization values of different nanoparticles; **(A)** iron nanoparticle, **(B)** core shell, and **(C)** pesticides loaded FMMIP.

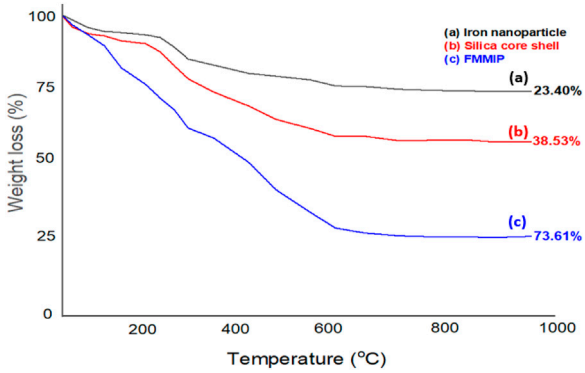

FIGURE 5
Thermogravimetric weight loss of: **(A)** iron nanoparticle, **(B)** core shell, and **(C)** pesticides loaded FMMIP.

organic materials (such as citrate groups from the synthesis process) and moisture. Additionally, an 8% weight reduction between 300°C and 500°C was observed due to the breakdown of labile oxygen groups, culminating in a total weight loss of 29%. The Fe_3O_4-SiO_2-FITC nanocomposite (Figure 5B) showed a significant weight decrease of around 36.87%, indicative of the decomposition of the silica and FITC layers. In contrast, the FMMIPs (Figure 5C) exhibited three distinct stages of weight loss: about 36% below 400°C

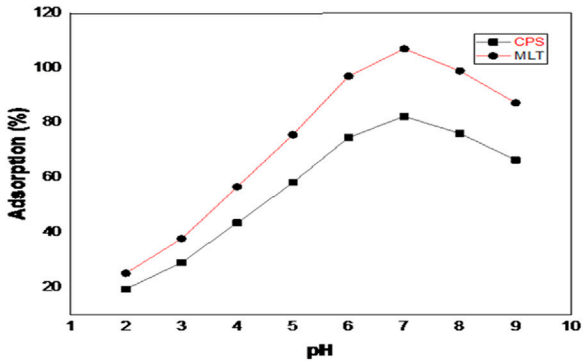

FIGURE 6
Effect of solution pH on adsorption MLT and CPS onto FMMIPs.

and 34% between 400°C and 600°C, which can be ascribed to the evaporation of adsorbed water and the degradation of the organic constituents of the crosslinker and the pesticides. These TGA results confirm the stability and composition of the nanomaterials, with the FMMIPs showing a higher weight loss due to the presence of additional organic layers (Liu et al., 2010).

3.5 pH influence on adsorption efficiency

The solution pH is a pivotal factor affecting target molecules' loading efficiency of MLT and CPS into the FMMIPs matrix. This phenomenon is primarily due to the pH-dependent electrostatic interactions between the adsorbent and the adsorbate (Oyetade et al., 2018). Adsorption experiments were conducted with 25 mg L^{-1} of each pesticide across a pH range of 2.0–9.0. Figure 6 graphically illustrates the effect of solution pH on the adsorption of MLT and CPS onto FMMIPs.

As depicted in this Figure, the adsorption rates of MLT and CPS on FMMIP increased with rising pH levels, peaking at pH 7.0. At this optimal pH, maximum adsorption was recorded at 96.5% for MLT and 88.3% for CPS and similar results were observed in previous studies (Dehghani et al., 2017). Since, dopamine is polymerized in slightly basic conditions so, its NH- and OH- groups becomes active to strongly bind with targets (MLT and CPS) in neutral to slightly alkaline conditions, allowing for effective and efficient binding. However, the self-polymerization of dopamine is hindered by acidic or highly alkaline environments, leading to changes in the polydopamine layer. These changes impact the surface interactions with the carrier and result in decreased adsorption capability (Ge et al., 2024). Figure 6 graphically illustrates the effect of solution pH on the adsorption of MLT and CPS onto FMMIPs.

3.6 Kinetic studies

In order, to assess the binding efficiency of FMMIP for MLT and CPS, kinetic studies were conducted. A series of experiments were conducted to obtain kinetic data at different time intervals followed by analysis of the data through pseudo-first-order and pseudo-second-order kinetic models (Figure 7; Table 1). These models are commonly used to study adsorption kinetics. The pseudo-first-order model assumes that the adsorption rate is proportional to the number of unoccupied sites. This model is used when the adsorbate concentration is low. The pseudo-second-order model assumes that the adsorption rate is proportional to the square of the number of unoccupied sites and is used when the adsorption process is more complex.

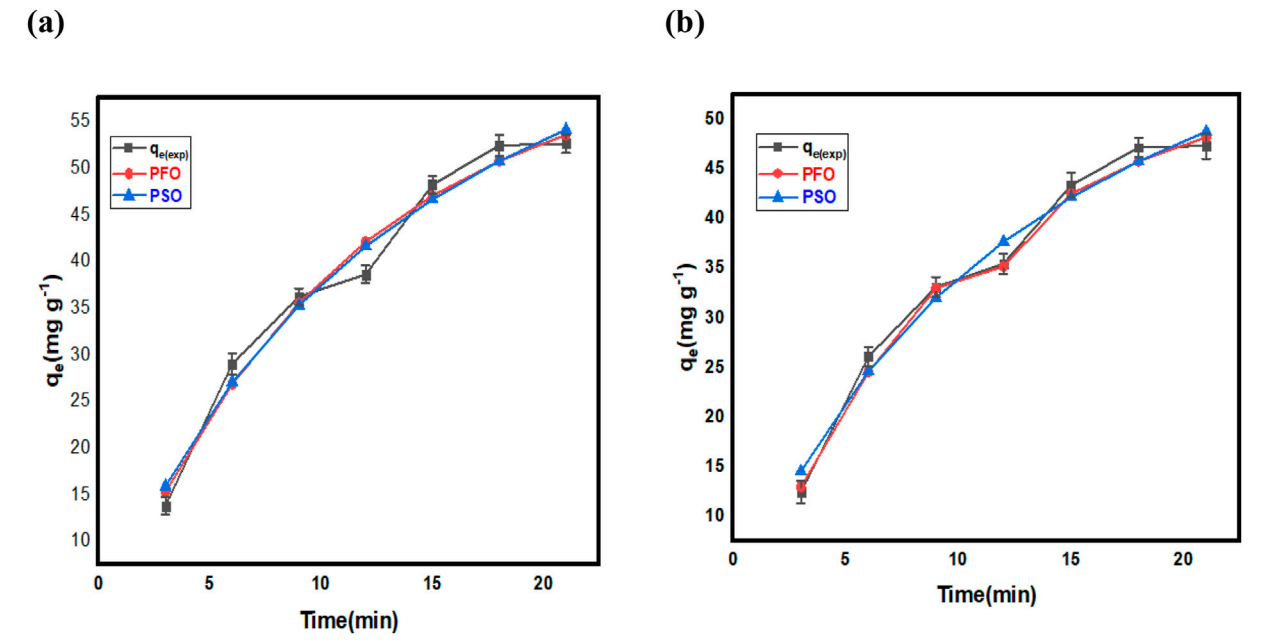

FIGURE 7
Non-linear fitting of PFO and PSO for pesticide adsorption on FMMIP; **(A)** MLT and **(B)** CPS pesticides.

TABLE 1 Adsorption kinetic parameters obtained using the PFO and PSO models for MLT and CPS on FMMIP.

	Pseudo-first - order					Pseudo - second - order					
	$q_{e,exp}$ (mg/g)	$q_{e,cal}$ (mg/g)	K_1	R^2	χ^2	$q_{e,cal}$ (mg/g)	K_2	$t_{1/2}$ (min)	h_0 mg/(g.min)	R^2	χ^2
MLT	54.2	62.2	0.094	0.9902	4.103	90.3	7.9 10^{-4}	14.0	6.44	0.9897	4.297
CPS	49.0	55.5	0.097	0.9919	2.754	80.3	9.2 10^{-4}	13.6	5.91	0.9909	3.057

Pseudo-First-Order Kinetic Model: The pseudo-first-order kinetic model is generally expressed by the Lagergren's rate equation (Equation 2):

$$q_t = q_e\left(1 - e^{-k_1 t}\right) \tag{2}$$

where q_e is the amount of adsorbate adsorbed at equilibrium (mg/g), q_t is the amount of adsorbate adsorbed at time t (mg/g), k_1 is the rate constant of pseudo-first-order adsorption (1/min), t is the time (min).

Pseudo-Second-Order Kinetic Model: The pseudo-second-order kinetic model, on the other hand, is represented by the following Equation 3:

$$q_t = k_2 q_e^2 t / \left(1 + k_2 q_e t\right) \tag{3}$$

Where k_2 is the rate constant of pseudo-second-order adsorption (g/mg min).

For both models, qe and qt are determined through experiments, and the rate constants k_1 and k_2 are estimate from the nonlinear forms of the respective equations against time t.

The initial adsorption rate (h_0) is defined as the rate at which the adsorbate is adsorbed at the beginning of the process when time approaches zero. For the pseudo-second-order kinetic model, the initial adsorption rate is given by Equation 4:

$$h_0 = k_2 q_e^2 \tag{4}$$

The half-life $t_{1/2}$ of an adsorption process is the time required for half of the adsorbate to be adsorbed onto the adsorbent. For the pseudo-second-order model, the half-life is given by Equation 5:

$$t_{\frac{1}{2}} = 1/k_2 q_e \tag{5}$$

The adsorption kinetics of MLT and (CPS) on FMMIP were elucidated using pseudo-first-order (PFO) and pseudo-second-order (PSO) kinetic models (See Figure 7). The estimated parameters of both kinetics models: the experimental (qexp) and calculated (qecal) adsorption capacities, rate constants (K1 for PFO and K2 for PSO), half-life (t1/2), initial adsorption rate (h0), and the fit quality parameters (R^2 and χ^2) are listed in Table 1 for both MLT and CPS.

The PFO model not only demonstrated high correlation coefficients (R^2) of 0.9902 for MLT and 0.9919 for CPS but also provided calculated equilibrium adsorption capacities ($q_{e,cal}$) of 62.2 mg/g for MLT and 55.5 mg/g for CPS, which closely approximate the experimentally observed values ($q_{e,exp}$) of 54.2 mg/g for MLT and 49.0 mg/g for CPS. These results and lower chi-square (χ^2) values of 4.103 and 2.754 exemplify a more precise fit than the PSO model. The PSO model permits the calculation of half-life ($t_{1/2}$) and initial adsorption rates (h_0). The half-life for MLT and CPS was determined to be 14.0 and 13.6 min, respectively, suggesting a rapid adsorption process. The initial adsorption rates (h_0) were 6.44 mg/(g.min) for MLT and 5.91 mg/(g.min) for CPS. The PSO model is more favorable due to its R^2 value being closer to 1, low χ^2 values, and the substantial agreement between the experimental and calculated q_e values, highlighting its relevance in modelling the adsorption behavior on FMMIP and providing a solid foundation for future process optimization and design (Hayat et al., 2024).

3.7 Adsorption isotherms

Understanding the equilibrium relationship between adsorbate concentrations and the binding capacity of an adsorbent at a set temperature is fundamental to adsorption isotherm studies. In this investigation, the Langmuir and Freundlich isotherm models were applied to interpret the experimental data acquired for the FMMIP. The Langmuir model presupposes the existence of homogenous monolayer binding sites across the adsorbent's surface with uniform adsorption energies. This model is described by Equation 6:

$$q_e = \frac{K_L q_m C_e}{1 + K_L C_e} \tag{6}$$

where q_e is the amount of adsorbate adsorbed (MLT or CPS) per unit mass of FMMIP, q_m indicates the maximum monolayer adsorption capacity of FMMIP, C_e is the equilibrium concentration of the adsorbate, and K_L is the Langmuir adsorption constant, which relates to the adsorption energy.

The dimensionless separation factor or equilibrium parameter, R_L, is calculated using Equation 7:

$$R_L = \frac{1}{1 + K_L C_0} \tag{7}$$

Conversely, the Freundlich isotherm model addresses heterogeneous surface binding sites with variable energies of adsorption, expressed as Equation 8:

$$q_e = K_F C_e^{1/n} \tag{8}$$

Here, K_F is the Freundlich adsorption constant related to the adsorption capacity, and n is the heterogeneity factor of the adsorption process.

The fitting of the experimental data to the Langmuir and Freundlich isotherm models was quantitatively assessed using the coefficient of determination (R^2) and the reduced Chi-square (χ^2). Figure 8 illustrates the FMMIP's adsorption capacity for MLT and CPS against the equilibrium concentration of the adsorbates. The Freundlich isotherm, marked by the red line, more accurately reflects the data for both substances than the Langmuir isotherm, represented by the blue line.

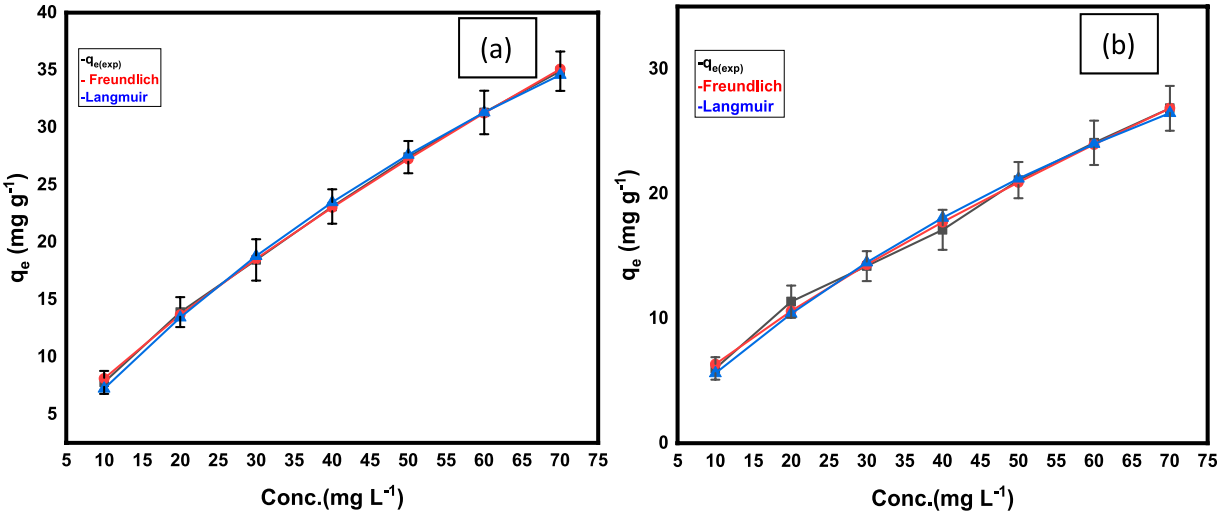

FIGURE 8
Langmuir and Freundlich Nonlinear models fitting of experimental adsorption data of **(A)** MLT and **(B)** CPS adsorption onto FMMIP.

TABLE 2 Adsorption isotherms parameters for MLT and CPS on FMMIP using the Langmuir and Freundlich models.

Sorbate	Langmuir					Freundlich			
	q_{ecal} (mg.g^{-1})	K_L (L.mol^{-1})	R_L (mg.g^{-1})	R^2	χ^2	K_f (L.g^{-1})	n	R^2	χ^2
MLT	93.52	0.0084	0.6297	0.9983	0.187	1.4334	1.329	0.9996	0.0486
CPS	69.74	0.0087	0.6204	0.9931	0.451	1.4343	1.346	0.9965	0.2246

Corresponding to the higher R^2 values for the Freundlich isotherm reported in Table 2 (0.9996 for MLT and 0.9965 for CPS), the data points indicate a precise model alignment, confirming an exemplary fit. The Langmuir isotherm demonstrates slightly lower R^2 values (0.9983 for MLT and 0.9931 for CPS) alongside marginally higher reduced Chi-square (χ^2) values, underscoring a less accurate fit than the Freundlich model.

The adherence of the experimental data to the Freundlich model, as shown in Figure 8, suggests that a heterogeneous mechanism better describes the adsorption of MLT and CPS onto FMMIP. The model's alignment with the observed data supports the presence of varied binding sites on the FMMIP surface, which accommodate a non-uniform and multilayer adsorption, consistent with the nature of the Freundlich model.

The discrepancies between the Langmuir model and the empirical data, particularly noticeable at elevated equilibrium concentrations, highlight the shortcomings of its assumption of homogeneous adsorption sites and uniform binding energies for the adsorbates in question.

Further, discernment is gained from analyzing the Freundlich isotherm's "n" values—1.329 for MLT and 1.346 for CPS—both of which lie within the optimal range of 1–10, indicating advantageous adsorption. Values of "n" above one implies an increasing efficiency in adsorption as the adsorbate concentration rises due to the likely interactions with the surface.

In parallel, evaluating the Langmuir isotherm's dimensionless constant, *RL*, for MLT (0.6297) and CPS (0.6204) reveals values below one, signifying a favorable adsorption process despite the Freundlich model's superior fit. An *RL* value within the range of 0–1 is characteristic of good adsorption, suggesting an increased likelihood of adsorption with rising initial concentration until the saturation point is reached at q_m.

In the current study, the Freundlich isotherm demonstrated the best fit, as evidenced by its R^2 value being close to 1 and the experimental maximum q_e value closely adheres the calculated value. Additionally, the value of n greater than 1 further supports the suitability of the Freundlich model. These findings indicate that FMMIP is an effective adsorbent for MLT and CPS under the tested conditions (Hayat et al., 2023).

3.8 Regeneration study

The regeneration potential of the FMMIP was assessed for MLT and CPS through multiple adsorption-desorption cycles, gauging the polymer's applicability for repeated use in analytical applications. Initially, FMMIP demonstrated recoveries of 85.3% for CPS and 80.4% for MLT in the first cycle. There was a subtle decline in recovery efficiency throughout five cycles, with the fifth cycle showing 73.7% for CPS and 71.2% for MLT, as illustrated in Figure 9. These findings underscore the durable nature of FMMIP, confirming its utility and persistent performance for sequential analytical procedures, thereby indicating its considerable value for practical implementation in pollutant extraction.

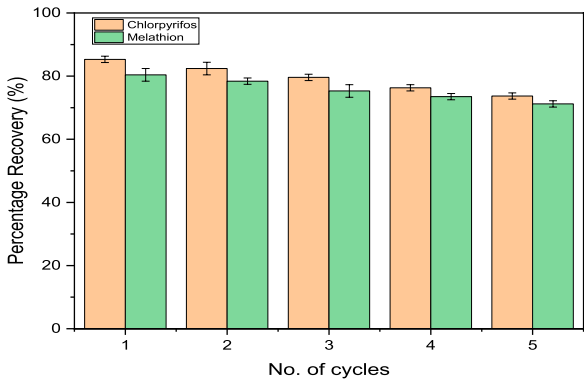

FIGURE 9
Regeneration studies of FMMIP for CPS and MLT.

3.9 Method validation through statistical analysis

Quality assurance (QA) parameters are essential in evaluating the selectivity and precision of MIP-based adsorption methods. These parameters encompass precision, linearity, the limit of detection (LOD), the limit of quantification (LOQ), and the relative standard deviation (RSD). Inter- and intra-day RSDs were calculated from measurements taken in the afternoon and then 1 week later to ascertain the precision of the developed method. The intra-day RSD values for MLT were 6.5% (n = 5), with an inter-day RSD of 7.1%. For CPS, the intra- and inter-day RSDs were 7.3% and 7.7%, respectively. Linearity was observed for both MLT and CPS within the 5–25 mg L^{-1} concentration range. The determined LOQs were 4 mg L^{-1} for MLT and 3.7 mg L^{-1} for CPS, while the LODs were calculated to be 1.26 mg L^{-1} for MLT and 1.22 mg L^{-1} for CPS. The calibration curves for MLT and CPS, as shown in Figures 10B,D, exhibited excellent regression values of 0.992 and 0.998, respectively, confirming the robustness and reliability of the method.

4 Conclusion

In this investigation, the development of a selective FMMIP was achieved, with a demonstrated proficiency for the extraction of MLT and CPS from agricultural Runoff. The meticulous characterizations, including TEM and TGA analyses, validated the integrity and successful synthesis of the FMMIP, with a noticeable polymer coating and significant thermal stability characterized by a 73.61% weight loss upon heating. Magnetic evaluations showed the FMMIP to possess a magnetization of 0.006 emu/g, confirming its ease of separation under an external magnetic field.

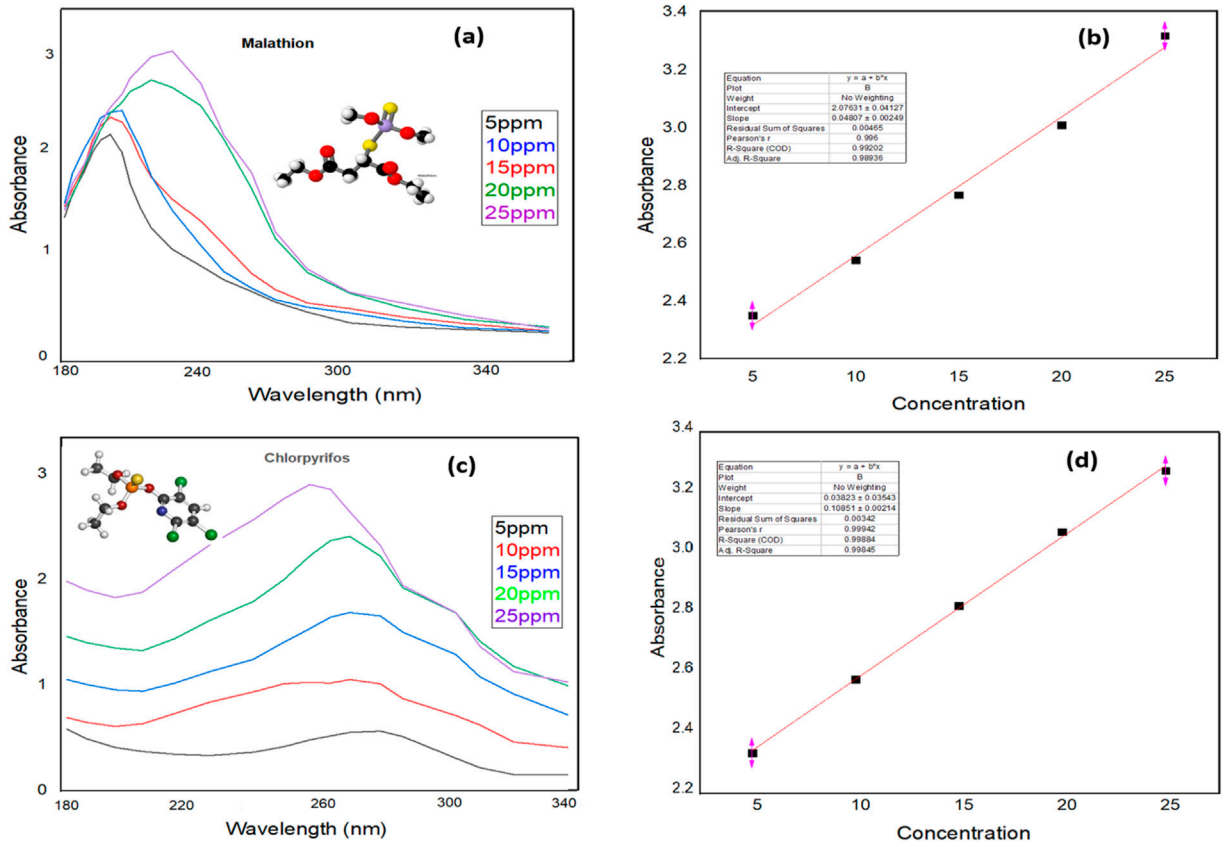

FIGURE 10
Absorption spectra and calibration curves of MLT and CPS: **(A)** absorption spectra of MLT, **(B)** calibration curve of MLT, **(C)** absorption spectra of CPS, and **(D)** calibration curve of CPS.

The high adsorption capacities of FMMIP 93 mg/g for MLT and 69 mg/g for CPS demonstrate its effectiveness in capturing and removing pesticides from agricultural runoff. The observed excellent performance in multiple regeneration cycles (with minimal efficiency loss) reflects the robust interaction between the pesticide molecules and the FMMIP surface, as well as the stability of the material under repeated use. These physicochemical processes, including the presence of heterogeneous binding sites and the physisorption nature of the interaction, are key factors that govern pesticide removal. Electrostatic forces primarily govern the interactions between the pesticides and the synthesized nanomaterial, van der Waals interactions, and hydrogen bonding, all contributing to the material's high binding efficiency and capacity.

Statistical analysis provided further validation, with RSD values of 6.5% for MLT and 7.3% for CPS, alongside detection limits at 1.26 mg/L for MLT and 1.22 mg/L for CPS. The high coefficients of determination (R^2 values) of 0.992 for MLT and 0.998 for CPS strongly supported the method's validity.

In summary, the FMMIP represents a significant advancement in environmental remediation, offering a robust, efficient, and reusable solution for the selective extraction of hazardous pesticides. Its alignment with the pseudo-first-order kinetic model and Freundlich isotherm underscores the tailored interaction between the FMMIP and the pesticide molecules, enhancing its practical application for safeguarding ecosystems against agricultural pollutants.

Data availability statement

The original contributions presented in the study are included in the article/Supplementary Material, further inquiries can be directed to the corresponding authors.

Author contributions

ZA: Writing–original draft. NR: Writing–original draft. MH: Writing–review and editing. LK: Writing–review and editing. MK: Writing–review and editing, Funding acquisition. EA: Writing–review and editing. NB: Writing–review and editing. HP: Writing–review and editing, Validation, Funding acquisition. AC: Writing–original draft.

Funding

The author(s) declare that financial support was received for the research, authorship, and/or publication of this article. This work was supported and funded by the Deanship of Scientific Research at Imam Mohammad Ibn Saud Islamic University (IMSIU) (grant number IMSIU-RG23019).

Conflict of interest

The authors declare that the research was conducted in the absence of any commercial or financial relationships that could be construed as a potential conflict of interest.

Generative AI statement

The author(s) declare that no Generative AI was used in the creation of this manuscript.

Publisher's note

Supplementary material

The Supplementary Material for this article can be found online at: https://www.frontiersin.org/articles/10.3389/fnano.2024.1516133/full#supplementary-material

References

Akgönüllü, S., and Denizli, A. (2022). Molecular imprinting-based sensors: lab-on-chip integration and biomedical applications. *J. Pharm. Biomed. Anal.* 225, 115213. doi:10.1016/j.jpba.2022.115213

Ali, G. K., and Omer, K. M. (2022). Molecular imprinted polymer combined with aptamer (MIP-aptamer) as a hybrid dual recognition element for bio(chemical) sensing applications. *Talanta* 236, 122878. doi:10.1016/j.talanta.2021.122878

Ali, Z., Zhang, P., Fan, Z., Zhang, Z., Wang, X., Li, Y., et al. (2022). Biodegradable magnetic molecularly imprinted anticancer drug carrier for the targeted delivery of docetaxel. *ACS Omega* 7 (30), 28516–28524. doi:10.1021/acsomega.2c03299

Ali, Z., Sajid, M., Ahmed, M. M., Hanif, M., and Manzoor, S. (2024). Synthesis of green fluorescent cross-linked molecularly imprinted polymer bound with anti-cancerous drug (docetaxel) for targented drug delivery. *Polym. Bull.* 81 (1), 679–696.

Ansari, S., and Karimi, M. (2017). Recent configurations and progressive uses of magnetic molecularly imprinted polymers for drug analysis. *Talanta* 167, 470–485. doi:10.1016/j.talanta.2017.02.049

Asadi, E., Pilehvar, S., Asghari, M., Omidi, M., Wilson, J. N., and Azodi-Deilami, S. (2016). *In vitro/in vivo* study of novel anti-cancer biodegradable cross-linked tannic acid for fabrication of 5-fluorouracil-targeting drug delivery nano-device based on a molecular imprinted polymer. *RSC Adv.* 6 (47), 37308–37318. doi:10.1039/c6ra03704f

Assafi, A., Ali, Y. A. E. H., Almufarij, R. S., Hejji, L., Raza, N., Villarejo, L. P., et al. (2023). Ultrasound-assisted adsorption of organic dyes in real water samples using zirconium (IV)-based metal-organic frameworks UiO-66-NH2 as an adsorbent. *Heliyon* 9, e22001. doi:10.1016/j.heliyon.2023.e22001

Ata, S., Akhtar, M., Rashid, N., Wattoo, M., Tirmizi, S., and Asad, M. (2013). Analytical investigation of selected pesticide residues from fruits and vegetables by an improved extraction method using reverse phase high performance liquid chromatograph. *Ethiop. J. Environ. Stud. Manag.* 6 (3), 342–347. doi:10.4314/ejesm.v6i4.1

Bharti, S., and Rasool, F. (2021). Analysis of the biochemical and histopathological impact of a mild dose of commercial malathion on *Channa punctatus* (Bloch) fish. *Toxicol. Rep.* 8, 443–455. doi:10.1016/j.toxrep.2021.02.018

Bojdi, M. K., Saraji, M., Rouhani, M., and Youssefi, S. (2016). Application of magnetic lamotrigine-imprinted polymer nanoparticles as an electrochemical sensor for trace determination of lamotrigine in biological samples. *RSC Adv.* 6 (33), 32374–32380. doi:10.1039/c6ra02096h

Coria, J., and Elgueta, S. (2022). Towards safer use of pesticides in Chile. *Environ. Sci. Pollut. Res.* 29 (17), 22785–22797. doi:10.1007/s11356-022-18843-6

Dehghani, M. H., Niasar, Z. S., Mehrnia, M. R., Shayeghi, M., Al-Ghouti, M. A., Heibati, B., et al. (2017). Optimizing the removal of organophosphorus pesticide malathion from water using multi-walled carbon nanotubes. *Chem. Eng. J.* 310, 22–32. doi:10.1016/j.cej.2016.10.057

Dhananjayan, V., Ashokkumar, L., Selvan, R., and Rao, R. R. (2020). "Agrochemicals impact on ecosystem and bio-monitoring," in *Resources use efficiency in agriculture* (Cham, Switzerland: Springer), 349–388. doi:10.1007/978-3-030-48841-0_14

Encarnação, T., Pais, A. A., Campos, M. G., and Burrows, H. D. (2019). Endocrine disrupting chemicals: impact on human health, wildlife, and the environment. *Sci. Prog.* 102, 3–42. doi:10.1177/0036850419826802

Ge, Y., Ding, L., Liu, Y., and Li, X. (2024). Synthesis, characterization and evaluation of a pH-responsive molecular imprinted polymer for Matrine as an intelligent drug delivery system. *e-Polymers* 24, 20230184. doi:10.1515/epoly-2023-0184

Gul, S., Gul, H., Raza, N., Azzouz, A., Elamin, M. R., Khezami, L., et al. (2024). Enhanced adsorptive removal of malachite green in environmental samples using Java plum leaves: from equilibrium to mechanism studies. *Biomass Convers. Biorefinery*, 1–17.

Han, Y., Zhao, Q., Song, Y., Lu, C., Sun, Z., and Yang, W. (2022). Molecularly imprinted polymers as the epitome of excellence in multiple fields. *Eur. Polym. J.* 169, 111582. doi:10.1016/j.eurpolymj.2022.111582

Hasanah, A. N., Wahyuni, W. T., Zulfikar, M. A., Neli, N., and Rahayu, D. (2021). Factors affecting preparation of molecularly imprinted polymer and methods on finding template-monomer interaction as the key of selective properties of the materials. *Molecules* 26 (18), 5612. doi:10.3390/molecules26185612

Hashimi, M. H., Hashimi, R., and Ryan, Q. (2020). Toxic effects of pesticides on humans, plants, animals, pollinators, and beneficial organisms. *APRJ* 5 (1), 37–47. doi:10.9734/aprj/2020/v5i430114

Hayat, M., Manzoor, S., Raza, H., Khan, M. I., Shanableh, A., Sajid, M., et al. (2023). Molecularly imprinted ormosil as a sorbent for targeted dispersive solid phase micro extraction of pyriproxyfen from strawberry samples. *Chemosphere* 320, 137835. doi:10.1016/j.chemosphere.2023.137835

Hayat, M., Manzoor, S., Raza, N., Raza, H., Javed, A., Ali, Z., et al. (2024). Amine-functionalized organically modified silica for the effective adsorption of Chlorpyrifos and Triazophos Residues from Orange juice. *Food Chem.* 141967. doi:10.1016/j.foodchem.2024.141967

Kralj, S., Makovec, D., and Drofenik, M. (2010). Producing ultra-thin silica coatings on iron-oxide nanoparticles to improve their surface reactivity. *J. Magnetism Magnetic Mater.* 322 (12), 1847–1853. doi:10.1016/j.jmmm.2009.12.038

Liu, H., Cupp, E. W., Guo, A. G., and Liu, N. (2004). Insecticide resistance and cross-resistance in Alabama and Florida strains of *Culex quinquefasciatus*. *J. Med. Entomology* 41 (3), 408–413. doi:10.1603/0022-2585-41.3.408

Liu, J., Shen, X., Li, Y., and Xu, H. (2010). "Removal of chlorpyrifos from contaminated water using molecularly imprinted polymeric microspheres," in *Proceedings of the 2010 4th International Conference On Bioinformatics and Biomedical Engineering (iCBBE)* (Chengdu, China: IEEE), 1–4.

Monsalve-Atencio, R., Montaño, D. F., and Contreras-Calderón, J. (2022). Molecular imprinting technology and poly (ionic liquid)s: promising tools with industrial application for the removal of acrylamide and furanic compounds from coffee and other foods. *Crit. Rev. Food Sci. Nutr.* 63, 6820–6839. doi:10.1080/10408398.2022.2038078

Mrozek, R. A., Singh, P., Hadjichristidis, N., Chremos, A., Kosan, D. J., Hedden, R. C., et al. (2010). Design of nonaqueous polymer gels with broad temperature performance: impact of solvent quality and processing conditions. *J. Mater. Res.* 25 (6), 1105–1117. doi:10.1557/jmr.2010.0155

Oyetade, O. A., Martincigh, B. S., and Skelton, A. A. (2018). Interplay between electrostatic and hydrophobic interactions in the pH-dependent adsorption of ibuprofen onto acid-functionalized multiwalled carbon nanotubes. *J. Phys. Chem. C* 122, 22556–22568. doi:10.1021/acs.jpcc.8b06841

Rahman, H. U., Waseem, M., Khan, M. R., Ali, S., Ahmed, A., and Khalid, N. (2021). A comprehensive review on chlorpyrifos toxicity with special reference to endocrine disruption: evidence of mechanisms, exposures, and mitigation strategies. *Sci. Total Environ.* 755, 142649. doi:10.1016/j.scitotenv.2020.142649

Rey, J. R., O'Meara, G. F., O'Connell, S. M., Carbis, H., O'Connell, S., Berg, J., et al. (2012). North American wetlands and mosquito control. *Int. J. Environ. Res. Public Health* 9 (12), 4537–4605. doi:10.3390/ijerph9124537

Sharma, R. K., Agarwal, A., Durairajanayagam, D., and Sharma, P. (2020). Insecticides and ovarian functions. *Environ. Mol. Mutagen.* 61 (3), 369–392. doi:10.1002/em.22355

Urucu, O. A., Çiğil, A. B., Birtane, H., Yetimoğlu, E. K., and Kahraman, M. V. (2020). Selective molecularly imprinted polymer for the analysis of chlorpyrifos in water samples. *J. Industrial Eng. Chem.* 87, 145–151. doi:10.1016/j.jiec.2020.03.025

Villa, C. C., Landero, I., Nieto, R. M., Villa, R. G., and Gutiérrez, T. J. (2021). Molecularly imprinted polymers for food applications: a review. *Trends Food Sci. Technol.* 111, 642–669. doi:10.1016/j.tifs.2021.03.003

Yin, Y., Zhang, B., Zhao, G., Luo, X., and Zhu, L. (2015). Magnetic molecularly imprinted polydopamine nanolayer on multiwalled carbon nanotubes surface for protein capture. *Talanta* 144, 671–679. doi:10.1016/j.talanta.2015.06.067

Zarei, M., and Zarei, M. (2018). Self-propelled micro/nanomotors for sensing and environmental remediation. *Small* 14 (20), 1800912. doi:10.1002/smll.201800912

Zuo, H. G., Zhu, J. X., Zhan, C. R., Shi, L., Xing, M., Guo, P., et al. (2015). Preparation of malathion MIP-SPE and its application in environmental analysis. *Environ. Monit. Assess.* 187, 394–419. doi:10.1007/s10661-015-4641-0